1,3-Dipolar Cycloaddition

Deutsche Ausgabe: DOI: 10.1002/ange.201501957
Internationale Ausgabe: DOI: 10.1002/anie.201501957

Region-Selective Deposition of Core–Shell Nanoparticles for 3D Hierarchical Assemblies by the Huisgen 1,3-Dipolar Cycloaddition**

Sebastian H. Etschel, Luis Portilla, Johannes Kirschner, Martin Drost, Fan Tu, Hubertus Marbach, Rik R. Tykwinski, and Marcus Halik**

Abstract: *A method for the region-selective deposition of nanoparticles (NPs) by the Huisgen 1,3-dipolar cycloaddition is presented. The approach enables defined stacking of various oxide NPs in any order with control over layer thickness. Thereby the reaction is performed between a substrate, functionalized with a self-assembled monolayer of an azide-bearing phosphonic acid (PA) and aluminum oxide (AlO_x) NPs functionalized with an alkyne bearing PA. The layer of alkyne functionalized AlO_x NPs is then used as substrate for the deposition of azide-functionalized indium tin oxide (ITO) NPs to provide a binary stack. This progression is then conducted with alkyne-functionalized CeO_2 NPs, yielding a ternary stack of NPs with three different NP cores. The stacks are characterized by AFM and SEM, defining the region-selectivity of the deposition technique. Finally, these assemblies have been tested in devices as a dielectric to form a capacitor resulting in a dramatic increase in the measured capacitance.*

The deposition of functional films and three-dimensional (3D) stacks with precise control in thickness and region-selectivity is a key enabler in smart processing for future thin-film electronics.[1] Thereby materials with different properties (for example, conductor, semiconductor, and insulator) are accessible as nanoparticles (NPs) but need to be carefully arranged to create functional devices. Self-assembly is a promising and elegant concept for the cost-effective, highly reproducible, and exceptionally selective assembly of materials in general.[2,3] The development of self-assembly of nanoparticles as a universal concept for the formation of hierarchical 3D structures would therefore represent a significant advance in device formation.[3] Since the Huisgen 1,3-dipolar cycloaddition, also often referred to as copper-catalyzed alkyne–azide cycloaddition (CuAAC) or simply click reaction was first introduced in 2001 by the groups of Sharpless and Médal, the reaction turned out to be a highly versatile method in the field of materials science.[4–8] In 2004, it was demonstrated that the click reaction can be used for the immobilization of functional materials on self-assembled monolayer (SAM) substrates,[9,10] and this concept has been quickly adapted to the field of surface chemistry.[11–13] Recently the CuAAC was performed with NPs, capped with a reactive organic monolayer of functionalized SAMs on flat substrates.[14–16] These so-called core–shell NPs offer huge potential regarding the ability to vary composition and electronic properties.[17] To our knowledge, however, the use of the CuAAC with core–shell systems and flat substrates has never been carried out region-selectively, or "location-selectively",[18] and with defined multilayer formation. The approach we present herein combines the universal applicability of the CuAAC with the versatility of inorganic–organic core–shell NPs to provide an efficient and region-selective deposition technique. We demonstrate a concept for precise region-selective film formation with control in film thickness and full control of the order of the materials in the formed 3D stacks, based on digital chemical selection of functionalized NPs.

Our approach for the region-selective deposition of the core–shell NPs is summarized in Figure 1. As the substrate, a bare aluminum oxide (AlO_x) surface **i**, grown on a Si wafer by an atomic layer deposition (ALD) process, was pre-patterned in the first step (step a, Figure 1; for details, see the Supporting Information). Substrate **ii** now features defined areas of two SAMs: the semi-fluorinated phosphonic acid (PA) **1** (green) and the azide-terminated PA **2** (blue) in a collinear, well-defined pattern. Whereas PA **2** promotes the CuAAC to the core–shell NPs (Scheme 1), the fluorinated PA **1** provides an effective passivation for inhibiting undesired aggregation of NPs next to the azide patterns. The strong chemical contrast of the two PAs on the surface of substrate **ii** is crucial for the region-selective deposition. The core–shell

[*] S. H. Etschel, Prof. Dr. R. R. Tykwinski
Department für Chemie und Pharmazie & Interdisciplinary Center for Molecular Materials (ICMM)
Friedrich-Alexander Universität Erlangen-Nürnberg (FAU)
Henkestrasse 42, 91054 Erlangen (Deutschland)
E-mail: rik.tykwinski@fau.de
Homepage: http://www.chemie.uni-erlangen.de/tykwinski

S. H. Etschel, L. Portilla, J. Kirschner, Prof. Dr. M. Halik
Department Werkstoffwissenschaften, Lehrstuhl für Polymerwerkstoffe, Organic Materials and Devices (OMD)
Friedrich-Alexander Universiät Erlangen-Nürnberg (FAU)
Martensstrasse 7, 91058 Erlangen (Deutschland)
E-mail: marcus.halik@fau.de
Homepage: http://omd.fau.de

M. Drost, F. Tu, Priv.-Doz. Dr. H. Marbach
Department für Chemie und Pharmazie
Lehrstuhl für Physikalische Chemie II
Friedrich-Alexander Universität Erlangen-Nürnberg (FAU)
Egerlandstrasse 3, 91058 Erlangen (Deutschland)
Homepage: https://www.chemie.uni-erlangen.de/dcp/forschung/arbeitskreise/arbeitskreis-marbach/

[**] This work was supported by the Cluster of Excellence Engineering of Advanced Materials (EAM) funded by the Deutsche Forschungsgemeinschaft (DFG), the Graduate School Molecular Science (GSMS), and the Graduate School 1161 "Disperse Systems for Electronic Applications".

Supporting information for this article is available on the WWW under http://dx.doi.org/10.1002/anie.201501957.

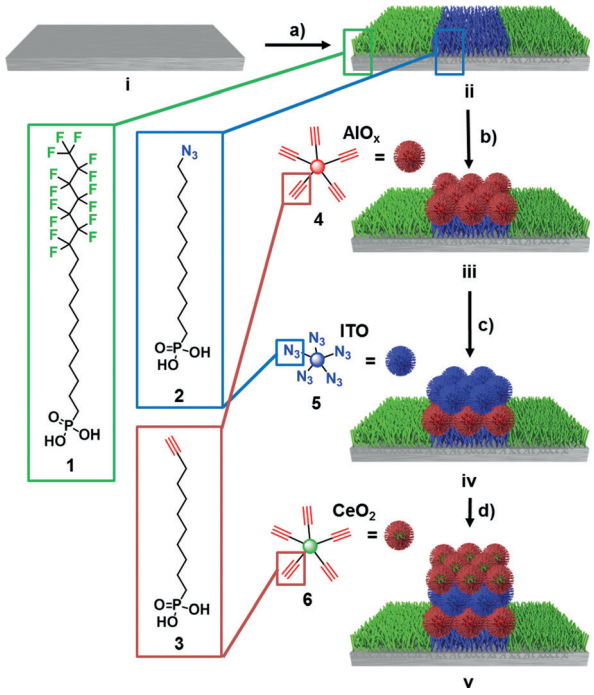

Figure 1. Outline for the region-selective deposition of NP assemblies for substrates **iii**–**v**; step a) pre-patterning of atomic layer deposition AlO_x substrate **i**; steps b–d) CuAAC according to Scheme 1.

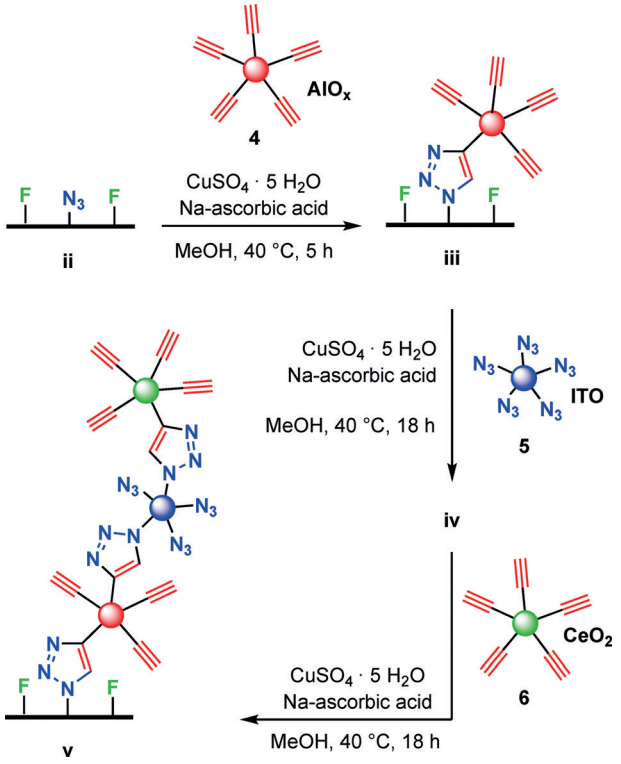

Scheme 1. CuAAC for the fabrication of substrates **iii**–**v** by assembling core–shell NPs **4**–**6**.

NPs required for step b were fabricated by a technique previously reported by our group.[19] The method enables easy access to azide- and alkyne-terminated NPs by choosing corresponding PA molecules **2** or **3**, respectively. Alkyne terminated PA **3** was grafted onto the AlO_x core, leading to NPs **4**. These NPs undergo the CuAAC with the azide headgroup of PA **2** on substrate **ii** (step b, Figure 1; Scheme 1). The result is the region-selectively deposited layer of NPs **4** on substrate **ii** to give **iii**. The second layer used indium tin oxide (ITO) NPs **5** that had been functionalized with azide terminated PA **2**, that is, the reactive counterpart of NP **4**. As a result, deposition of NPs **5** subsequently resulted in a click reaction with the unreacted alkyne groups of **4** from the first NP layer of substrate **iii** (step c, Figure 1). The resulting substrate **iv** is thus composed of a layer of ITO NPs **5** on top of the layer of AlO_x NPs **4**. The unreacted azide headgroups in the layer of ITO NPs **5** of substrate **iv** were subjected to a third CuAAC with again alkyne functionalized CeO_2 NPs **6** (step d, Figure 1, Scheme 1). The obtained substrate **v** features a defined ternary layered stack of selectively deposited core–shell NPs with three different cores (AlO_x, ITO, and CeO_2). The respective cores were chosen because they represent typical model systems (AlO_x[19,20]), high-performance materials (ITO[21]), or are promising candidates for various possible applications ranging from catalysis and optics, to electronics (CeO_2[22]). To establish the successful CuAAC under the applied conditions, the decrease of the azide band in the infrared was monitored by FTIR spectroscopy of dried NP powder (Supporting Information).[9,10,19]

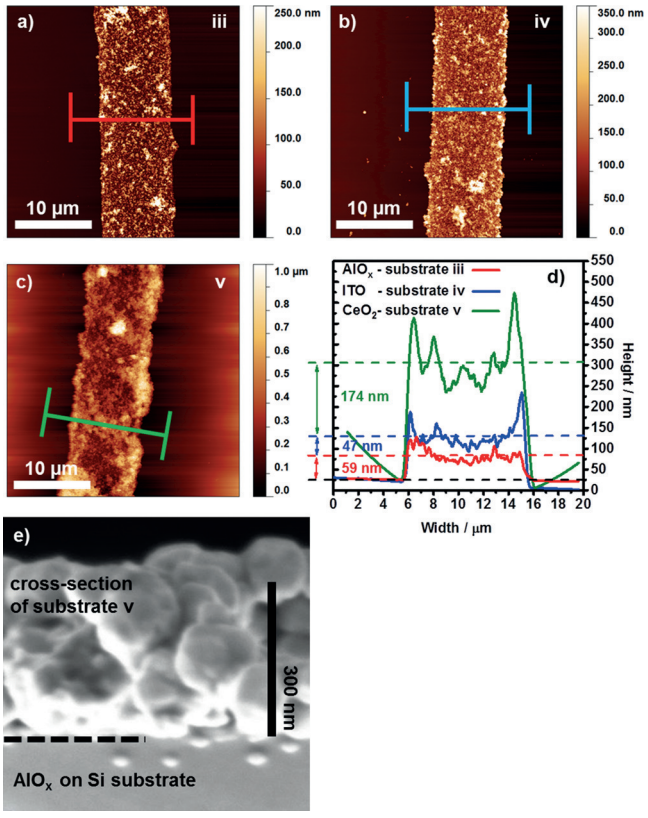

Figure 2. AFM scans of substrates a) **iii**, b) **iv**, and c) **v**; d) extracted height profiles of substrates **iii**–**v** plotted against each other and RMS horizontal fits as dashed lines; e) SEM cross-section of substrate **v** composed of AlO_x, ITO, and CeO_2 layers.

Atomic force microscopy (AFM) and scanning electron microscopy (SEM) are used to characterize the functionalized substrates. Figure 2a–c present the AFM scans of substrates **iii**–**v** and a comparison of the corresponding height profiles (Figure 2d). The mean diameter of the particles **4** (55 nm ±19 nm), **5** (56 nm ±16 nm), and **6** (66 nm ±20 nm) was determined by dynamic light scattering (DLS, see the Supporting Information). Figure 2a shows substrate **iii** with AlO_x NPs **4** assembled as the first layer, revealing a nearly perfect region-selectivity of the layer of the NPs. The reacted area in the middle of Figure 2a was prior patterned with azide terminated PA **2**. Only this activated region underwent the CuAAC reaction with alkyne functionalized NPs **4**. The areas without particles to the left and the right of the stripe pattern were passivized with semi-fluorinated PA **1**, which prevented the adsorption and precipitation of **4** to these spots. The extracted height profile is indicated by the red bar in Figure 2a and plotted as the red trace in Figure 2d. The overall layer thickness is close to a monolayer, regarding the mean NP diameter of about 55 nm for **4**. Owing to the homogeneous shell composition and the relatively dense packaging of the first NP layer, the surface is now inverted (according to CuAAC reaction mode) and supports the reactive alkyne groups that are available to react with the azide-terminated ITO NPs **5**. Figure 2b shows the AFM scan of substrate **iv** after functionalization with ITO NPs **5** as the second layer. It can be clearly seen that the ITO NPs were selectively deposited on top of the AlO_x NPs from the first layer. The blue bar indicates the point where the height profile was extracted and is plotted as blue trace in Figure 2d. The increase in layer thickness from the first (red trace) to the second layer (blue trace) is again in accordance as to what is expected from the mean diameter of ITO NPs **5**, regarding their polydispersity (56 nm ±16 nm). The surface is now azide-terminated and again accessible for the alkyne component of the CuAAC, provided by NPs **6**. Figure 2c presents the AFM measurement of substrate **v**, on which CeO_2 NPs **6** have been added as the third layer. The increase in layer thickness is more than expected based on the NP mean diameter of **6** (66 nm ±20 nm). The thickness of the CeO_2 layer can be explained by the pronounced aggregation of the NPs under the reaction conditions, as observed empirically, and reported by others.[23] Nevertheless, the region-selectivity was admirably preserved during the entire assembly from the first to the third layer. Figure 2e depicts the cross-section (CS) SEM scan of substrate **v**, simply cleaved with a diamond tip, showing a densely packed and well-defined layer of NPs. The thickness based on the CS is in accordance to the AFM scan in Figure 2c and the height profile in Figure 2d (green trace). The SEM top view measurements of substrates **iii**–**v** are summarized in the Supporting Information. Local Auger electron spectroscopy (AES) was carried out on plain-view samples and provided evidence for the presence of the AlO_x, ITO, and CeO_2 particles on the corresponding samples **iii**–**v** (Supporting Information).

To investigate the general suitability of our process for the fabrication of electronic devices, and particularly the incorporation/deposition of electrodes, the particle films of substrates **iii**–**v** were integrated as dielectric layers in capacitor devices. Capacitors were chosen as a prototypical device owing to their rather simple architecture. For device construction, the NPs **4**–**6** need to be assembled between two electrodes, an Al bottom and an Au top electrode. Thus, SAMs **1** and **2** were applied to a substrate with lithographically patterned Al structures (see the Supporting Information). The deposition of the NPs **4**–**6** followed the same procedure according to the conditions stated in Scheme 1.

The capacitances (measured at 10 kHz) of the fabricated devices were plotted versus the applied voltage (Figure 3).

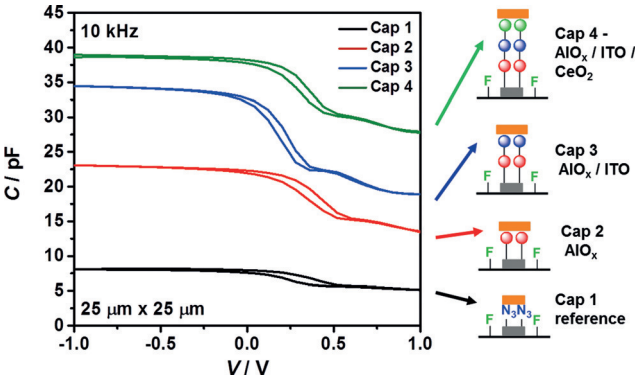

Figure 3. Capacitances of Cap **1**–**4** measured at 10 kHz switching frequency plotted against the applied potential; the area for all capacitors was 25 µm×25 µm.

Values measured at 500 kHz and 5 MHz are provided in the Supporting Information. Capacitor Cap **1** with a hybrid stack of AlO_x (created from O_2-plasma treated Al bottom electrode) and azide PA **2** SAM provides the reference (Figure 3, black trace). Device Cap **2** features AlO_x NPs **4**, assembled according to the CuAAC schematically shown in Scheme 1. The capacitance of devices Cap **2** increased upon loading them with AlO_x NPs **4** (Figure 3, red trace). This trend is further enhanced by the deposition of the ITO NPs **5** as the second layer (Cap **3**, blue trace) and CeO_2 NPs **6** as the third layer (Cap **4**, green trace). The increase in capacitance with increasing layer-thickness of the dielectric material is not expected for a typical plate capacitor (for a comparison, see the Supporting Information). However, the encapsulation of the inorganic core of the NPs **4**–**6** with a low-ε organic shell and the fact that NPs pack intrinsically less densely than the bulk material dramatically changes the electronic properties of the NP stacks, in comparison to the pristine material.[24] Furthermore, the organic capping of the NP cores leads to a strong frequency dependence of the measured capacitances (see the Supporting Information). It was observed that the capacitances dropped significantly by increasing the applied frequency. This phenomenon has been previously observed for particulate organic–inorganic hybrid materials.[25,26] A reason for the unexpected electronic behavior of the fabricated stacks might be pronounced charging of the assembled NP layers owing to the electronic shielding of the individual NPs by the organic shell.[27] Neither fabrication nor the performance of the capacitors has been optimized because this is outside the goals of the current study. Nevertheless, the

measured electronic characteristics are consistent over at least 4–5 measured devices in two independent series (Supporting Information). Thus, we demonstrate clearly that the 3D region-selective NP assembly by the CuAAC can be controlled, and the capacitors serve as a proof of concept for the fabrication of prototypical electronic devices.

In summary, we have presented a highly versatile solution-based process which allows the region-selective assembly of defined 3D structures on solid substrates by the Huisgen 1,3-dipolar cycloaddition. Specifically, core–shell NPs based on three different metal oxide cores were used for the spatially controlled assembly of a ternary stack of NPs. This general approach enables the arrangement of various materials with exquisite spatial resolution, and we demonstrate that this process can be easily adapted to contraction of electrical devices through the layer-by-layer formation of a capacitor.

Experimental Section

General Procedure for the CuAAC: Sodium ascorbate solution (13 mL, 5.0 mM in MeOH) was degassed with N_2 for 10 min. A solution of $CuSO_4 \cdot 5H_2O$ (0.64 mL, 5.0 mM in MeOH) was added under an N_2 inert atmosphere. The corresponding NPs **4**–**6** were then added as a dispersion (1 mL, 0.2 wt% in MeOH). The pre-patterned substrate **ii**, **iii**, or **iv** was immersed at the end. The mixture was stirred over the substrate for 5 h in the case of **4**, and for 18 h in the case of **5** and **6** at 40 °C under N_2 atmosphere. Afterwards, the substrate was taken out of the mixture, washed with MeOH once and *i*PrOH three times, and dried with N_2.

Keywords: 1,3-dipolar cycloaddition · nanoparticles · phosphonic acid · self-assembly · surface chemistry

How to cite: *Angew. Chem. Int. Ed.* **2015**, *54*, 9235–9238
Angew. Chem. **2015**, *127*, 9367–9370

[1] Y. Xia, G. M. Whitesides, *Angew. Chem. Int. Ed.* **1998**, *37*, 550–575; *Angew. Chem.* **1998**, *110*, 568–594.
[2] J. C. Love, L. A. Estroff, J. K. Kriebel, R. G. Nuzzo, G. M. Whitesides, *Chem. Rev.* **2005**, *105*, 1103–1170.
[3] M. J. Joralemon, R. K. O'Reilly, C. J. Hawker, K. L. Wooley, *J. Am. Chem. Soc.* **2005**, *127*, 16892–16899.
[4] M. Meldal, C. W. Tornøe, *Chem. Rev.* **2008**, *108*, 2952–3015.
[5] W. H. Binder, R. Sachsenhofer, *Macromol. Rapid Commun.* **2007**, *28*, 15–54.
[6] W. Xi, T. F. Scott, C. J. Kloxin, C. N. Bowman, *Adv. Funct. Mater.* **2014**, *24*, 2572–2590.
[7] C. W. Tornøe, C. Christensen, M. Méldal, *J. Org. Chem.* **2002**, *67*, 3057–3064.
[8] V. V. Rostovtsev, L. G. Green, V. V. Fokin, K. B. Sharpless, *Angew. Chem. Int. Ed.* **2002**, *41*, 2596–2599; *Angew. Chem.* **2002**, *114*, 2708–2711.
[9] J. P. Collman, N. K. Devaraj, C. E. D. Chidsey, *Langmuir* **2004**, *20*, 1051–1053.
[10] T. Lummerstorfer, H. Hoffmann, *J. Phys. Chem. B* **2004**, *108*, 3963–3966.
[11] R. A. Evans, *Aust. J. Chem.* **2007**, *60*, 384–395.
[12] C. Haensch, S. Hoeppener, U. S. Schubert, *Chem. Soc. Rev.* **2010**, *39*, 2323–2334.
[13] C. Nicosia, J. Huskens, *Mater. Horiz.* **2014**, *1*, 32–45.
[14] A. P. Upadhyay, D. K. Behara, G. P. Sharma, A. Bajpai, N. Sharac, R. Ragan, R. G. S. Pala, S. Sivakumar, *ACS Appl. Mater. Interfaces* **2013**, *5*, 9554–9562.
[15] I. Rianasari, M. de Jong, J. Huskens, W. van der Wiel, *Int. J. Mol. Sci.* **2013**, *14*, 3705–3717.
[16] J. Matyjewicz, A. Lesniewski, J. Niedziolka-Jonsson, *Electrochem. Commun.* **2014**, *48*, 73–76.
[17] H. Zhang, Y. Liu, D. Yao, B. Yang, *Chem. Soc. Rev.* **2012**, *41*, 6066–6088.
[18] P. Diao, M. Guo, Q. Hou, M. Xiang, Q. Zhang, *J. Phys. Chem. B* **2006**, *110*, 20386–20391.
[19] L. Portilla, M. Halik, *ACS Appl. Mater. Interfaces* **2014**, *6*, 5977–5982.
[20] G. Guerrero, J. G. Alauzun, M. Granier, D. Laurencin, P. H. Mutin, *Dalton Trans.* **2013**, *42*, 12569–12585.
[21] J. Ederth, P. Heszler, A. Hultåker, G. Niklasson, C. Granqvist, *Thin Solid Films* **2003**, *445*, 199–206.
[22] S. W. Depner, K. R. Kort, C. Jaye, D. A. Fischer, S. Banerjee, *J. Phys. Chem. C* **2009**, *113*, 14126–14134.
[23] S. Kar, C. Patel, S. Santra, *J. Phys. Chem. C* **2009**, *113*, 4862–4867; H. Gu, M. D. Soucek, *Chem. Mater.* **2007**, *19*, 1103–1110.
[24] Q. J. Cai, Y. Gan, M. B. Chan-Park, H. B. Yang, Z. S. Lu, Q. L. Song, C. M. Li, Z. Li Dong, *Appl. Phys. Lett.* **2008**, *93*, 113304.
[25] F.-C. Chen, C.-W. Chu, J. He, Y. Yang, J.-L. Lin, *Appl. Phys. Lett.* **2004**, *85*, 3295–3297.
[26] R. Schroeder, L. A. Majewski, M. Grell, *Adv. Mater.* **2005**, *17*, 1535–1539.
[27] U. Simon, *Adv. Mater.* **1998**, *10*, 1487–1492.

Received: March 2, 2015
Revised: April 27, 2015
Published online: June 18, 2015

